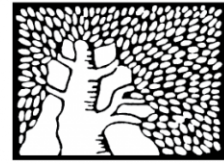


מכון ויצמן למדע

WEIZMANN INSTITUTE OF SCIENCE



Cancer-associated fibroblasts promote aggressive gastric cancer phenotypes via heat shock factor 1-mediated secretion of extracellular vesicles

Document Version:

Accepted author manuscript (peer-reviewed)

Citation for published version:

Grunberg, N, Pevsner-Fischer, M, Goshen-Lago, T, Diment, J, Stein, Y, Lavon, H, Mayer, S, Levi-Galibov, O, Friedman, G, Ofir-Birin, Y, Syu, L-J, Migliore, C, Shimoni, E, Stemmer, SM, Brenner, B, Dlugosz, AA, Lyden, D, Regev-Rudzki, N, Ben-Aharon, I & Scherz-Shouval, R 2021, 'Cancer-associated fibroblasts promote aggressive gastric cancer phenotypes via heat shock factor 1-mediated secretion of extracellular vesicles', *Cancer Research*, vol. 81, no. 7, pp. 1639-1653. <https://doi.org/10.1158/0008-5472.CAN-20-2756>

Total number of authors:

20

Digital Object Identifier (DOI):

[10.1158/0008-5472.CAN-20-2756](https://doi.org/10.1158/0008-5472.CAN-20-2756)

Published In:

Cancer Research

License:

Other

General rights

© 2020 This manuscript version is made available under the above license via The Weizmann Institute of Science Open Access Collection is retained by the author(s) and / or other copyright owners and it is a condition of accessing these publications that users recognize and abide by the legal requirements associated with these rights.

How does open access to this work benefit you?

Let us know @ library@weizmann.ac.il

Take down policy

The Weizmann Institute of Science has made every reasonable effort to ensure that Weizmann Institute of Science content complies with copyright restrictions. If you believe that the public display of this file breaches copyright please contact library@weizmann.ac.il providing details, and we will remove access to the work immediately and investigate your claim.

1 **Cancer-associated fibroblasts promote aggressive gastric cancer phenotypes via heat shock**
2 **factor 1-mediated secretion of extracellular vesicles**

3
4 Nil Grunberg¹, Meirav Pevsner-Fischer¹, Tal Goshen-Lago², Judith Diment³, Yaniv Stein¹, Hagar
5 Lavon¹, Shimrit Mayer¹, Oshrat Levi-Galibov¹, Gil Friedman¹, Yifat Ofir-Birin¹, Li-Jyun Syu⁴,
6 Cristina Migliore⁵, Eyal Shimoni⁶, Salomon M. Stemmer^{7,8}, Baruch Brenner^{7,8}, Andrzej A. Dlugosz^{4,9},
7 David Lyden¹⁰, Neta Regev-Rudzki¹, Irit Ben-Aharon^{2,11}, and Ruth Scherz-Shouval^{1*}

8
9 ¹Department of Biomolecular Sciences, The Weizmann Institute of Science, Rehovot, Israel

10 ²Division of Oncology, Rambam Health Care Campus, Haifa, Israel

11 ³Department of Pathology, Kaplan medical center. Rehovot, Israel

12 ⁴Department of Dermatology, Rogel Cancer Center, University of Michigan, Ann Arbor, MI, USA

13 ⁵ University of Torino, Department of Oncology, Candiolo; Candiolo Cancer Institute, FPO-IRCCS,
14 Candiolo, Italy

15 ⁶Department of Chemical Research Support, The Weizmann Institute of Science, Rehovot, Israel

16 ⁷Institute of Oncology, Davidoff Cancer Center, Rabin Medical Center, Beilinson Hospital, Petah
17 Tikva, Israel

18 ⁸Sackler Faculty of Medicine, Tel Aviv University, Ramat Aviv, Tel Aviv, Israel

19 ⁹Department of Cell & Developmental Biology, Rogel Cancer Center, University of Michigan, Ann
20 Arbor, MI, USA

21 ¹⁰Children's Cancer and Blood Foundation Laboratories, Departments of Pediatrics, and Cell and
22 Developmental Biology, Drukier Institute for Children's Health, Meyer Cancer Center, Weill Cornell
23 Medicine, New York, NY, USA

24 ¹¹Rappaport Faculty of Medicine, Technion, Haifa, Israel

25
26 *Correspondence should be addressed to R.S.S (Email: ruth.shouval@weizmann.ac.il)

27 **Running Title:** CAFs promote gastric cancer via HSF1 and exosomes

28 **Keywords:** gastric cancer, cancer-associated fibroblasts, HSF1, exosomes, tumor microenvironment

29 **Corresponding author:** Ruth Scherz-Shouval, Department of Biomolecular Sciences, The Weizmann
30 Institute of Science, Herzl 234 Rehovot, Israel, 76100, Tel +972-8-9342299, Fax +972-8-9344118,
31 Email: ruth.shouval@weizmann.ac.il

32
33 **Conflict of interest statement:** The authors declare that they have no conflict of interest.
34
35

36 **Abstract**

37 Gastric cancer is the 3rd most lethal cancer worldwide, and evaluation of the genomic status of gastric
38 cancer cells has not translated into effective prognostic or therapeutic strategies. We therefore
39 hypothesize that outcomes may depend on the tumor microenvironment (TME), in particular, cancer-
40 associated fibroblasts (CAF). However, very little is known about the role of CAFs in gastric cancer.
41 To address this, we mapped the transcriptional landscape of human gastric cancer stroma by
42 microdissection and RNA sequencing of CAFs from gastric cancer patients. A stromal gene signature
43 was associated with poor disease outcome, and the transcription factor heat shock factor 1 (HSF1)
44 regulated the signature. HSF1 upregulated inhibin subunit beta A (INHBA) and thrombospondin 2
45 (THBS2), which were secreted in CAF-derived extracellular vesicles (EV) to the TME to promote
46 cancer. Together, our work provides the first transcriptional map of human gastric cancer stroma and
47 highlights HSF1 and its transcriptional targets as potential diagnostic and therapeutic targets in the
48 genomically stable tumor microenvironment.

49

50 **Significance**

51 We highlight a stromal transcriptional program associated with aggressive gastric cancer, describe a
52 role for HSF1 in regulating it, and propose that this program is communicated to cancer cells via
53 exosome-mediated signaling.

54

55 **Introduction**

56 Gastric cancer is the 5th most common cancer and the 3rd most lethal cancer, worldwide (1). Recent
57 advances in treatment were made possible due to better classification of gastric cancer subtypes, but
58 the prognosis of advanced gastric cancer remains poor and many patients get diagnosed at an advanced
59 stage of the disease due to limited understanding of the underlying biology (2). There is an urgent need
60 to better understand the molecular basis of this disease, and to identify biomarkers that may predict
61 outcome and guide therapy.

62 Gastric cancer is a heterogeneous disease. Traditionally, anatomical location (true gastric vs gastro-
63 esophageal) and histological characteristics (diffuse vs intestinal; tubular vs papillary) have been used
64 to classify gastric cancer subtypes (2). Recent advances in molecular understanding have enabled
65 classification of gastric cancer into different subtypes based on chromosomal instability, microsatellite
66 instability, genomic stability, presence of Epstein-Barr virus, and epithelial- mesenchymal transition
67 (EMT), which were associated with different survival outcomes (3-6). Mutations in *CDHI* and *KRAS*,
68 and overexpression of HER2, EGFR, FGFR2, VEGF, were shown to contribute to disease progression
69 and correlate with poor outcome (7,8). Despite serving as valuable guides in deciphering the

70 complexity of gastric cancer, there has been little success in applying these molecular classifiers to
71 treatment stratification and development of targeted therapies (3). Prognosis in the clinic is still mostly
72 evaluated based on TNM staging (Tumor size, lymph Node involvement and Metastasis), and the
73 standard of care for localized gastric cancer is surgical intervention combined with chemotherapy (7).
74 Increasing evidence over the past decade highlighted the indispensable contribution of the tumor
75 microenvironment (TME) to disease progression and treatment resistance (9). The TME is comprised
76 of various cell types, including endothelial cells, fibroblasts, macrophages, and lymphocytes, as well
77 as extracellular matrix components (ECM) (10). The immune microenvironment of gastric cancer has
78 gained increasing attention over the last years, due to its potential effect on immunotherapy in patients
79 with high microsatellite instability (11). Yet little is known about the contribution of cancer-associated
80 fibroblasts (CAFs) to gastric cancer progression and metastasis. CAFs are the most abundant cell type
81 in a variety of carcinomas (12). They support cancer cells by modifying the ECM, promoting
82 angiogenesis and maintaining a chronic inflammatory state (12-17). In gastric cancer, accumulation of
83 CAFs is correlated with increased tumor size, invasion and metastasis (18). Recently, the abundance
84 of natural killer cells, endothelial cells and CAFs was shown to predict chemotherapy benefit in gastric
85 cancer (19). However, the specific genes and molecular events contributing to these protumorigenic
86 effects are not well understood. To address this, we set out to map the transcriptional landscape of
87 gastric CAFs. Using laser-capture microdissection (LCM) and RNA-sequencing of CAFs from gastric
88 cancer patients we define a gene-signature associated with poor disease outcome. We characterize this
89 signature using mouse models and co-culture assays, and show that components of this signature are
90 regulated by the master transcriptional regulator heat shock factor 1 (HSF1) (20), and secreted from
91 CAFs via extracellular vesicles (EVs). These fibroblast-derived EVs contribute to tumor growth in an
92 HSF1-dependent manner. Together, our work provides a comprehensive map of gastric cancer stromal
93 transcription with potential implications on prognosis and treatment.

94

95 **Materials and Methods**

96 **Ethics statement**

97 Clinical samples and patient data were collected following approval by the Rabin medical center
98 Institutional Review Board (IRB, protocol #0297-11-RMC) with full exemption for consent form for
99 anonymized samples. Human samples used for MxIF staining were obtained from the Israel National
100 Biobank for Research (MIDGAM; <https://www.midgam.org.il/>) under IRB # 6141-19-SMC. These
101 samples were collected from patients who provided written informed consent for collection, storage,
102 distribution of samples and data for use in future research studies. All animal studies were approved

103 by the Institutional Animal Care and Use Committee (IACUC protocol #15310619-2, #15140619-3,
104 #06690820-3).

105

106 **Mice**

107 Athymic Nude mice were purchased from Harlan biotech (Rehovot, Israel). These mice, the triple-
108 transgenic *Lgr5-EGFP-IRES-CreERT2; R26-LSL-rtTA-IRES-EGFP; tetO-GLI2A* mice, (*iLgr5;GLI2A*
109 mice (21)), *Hsf1* null mice and their WT littermates (BALB/c × 129SvEV, by Ivor J. Benjamin (22))
110 were maintained under specific-pathogen-free conditions at the Weizmann Institute's animal facility.

111

112 **Cell lines and primary cell cultures**

113 N87 gastric cancer cells were kindly provided by Yosef Yarden (WIS; originally from ATCC). N87
114 cells were transduced with green fluorescent protein (GFP) using a 3rd-generation lentiviral system.
115 MC38 colon cancer cells were kindly provided by Lea Eisenbach (WIS; originally from NCI). MC38
116 cells were transduced with mcherry-luciferase using a 2nd-generation lentiviral system. Primary MEFs
117 were produced from WT and *Hsf1* null mice. HFF cells were purchased from ATCC. MEFs, MC38
118 cells and N87 cells were cultured in RPMI (#01-100-1A, Biological Industries) supplemented with 10%
119 fetal bovine serum (FBS; Invitrogen) and P/S (Biological Industries). HFF cells were cultured in
120 DMEM (#01-052-1A, Biological Industries) supplemented with 15% FBS, 1.5% L-Glutamine and P/S.
121 Cell lines were tested routinely for *Mycoplasma* using EZ-PCR Mycoplasma test kit (#20-700-20,
122 Biological Industries). MEFs were used in passage 1. Other cell lines were maintained below passage
123 25.

124

125 **Laser capture microdissection of human gastric cancer samples**

126 LCM cohort patients were selected based on patient outcome data (Supplementary Table 1). Stromal
127 and cancer regions were marked by a trained pathologist blinded to clinical and outcome data to include
128 >90% CAFs for stroma and >90% cancer cells for cancer. Gastric muscle, immune islands, and blood
129 vessels were excluded from microdissection. FFPE slides were deparaffinized and stained using
130 Arcturus Paradise Plus Staining kit (#KIT0312J, Thermo-Fischer) according to the instructions of the
131 manufacturer. Slides were left to dry for 5 min at RT followed by microdissection using the Arcturus
132 (XT) laser microdissection instrument (#010013097, Thermo-Fischer). Infrared capture was used to
133 minimize RNA damage. CapSure Macro LCM caps (#LCM0211, Thermo-Fischer) were used to
134 capture microdissected tissue. To obtain sufficient material from these highly degraded RNA samples
135 we performed microdissection from 6-10, 5 µm sections per sample. Microdissected tissue from each
136 sample was pooled together, and kept on dry ice until RNA isolation using the RNeasy FFPE kit

137 (#73504, Qiagen) with one modification- proteinase K digestion at 56°C was carried out for 1 h.

138

139 **Library preparation, RNA-sequencing and analysis of LCM samples**

140 Libraries were prepared using the SMARTer Stranded Total RNA-Seq v2-Pico Input Mammalian kit
141 (#634415, Takara Bio USA) according to the instructions of the manufacturer. Libraries were
142 sequenced on Illumina NextSeq 500, at 50M reads for stroma and 25M reads for cancer samples, to
143 provide sufficient reads to pass quality control filters of RNA-seq. Principal Component Analysis
144 (PCA) was performed on full RNA-seq datasets for each sample (for stroma and cancer samples,
145 separately). After calculating the first 3 main PCs (PCA1-3), we used the Robust Mahalanobis distance
146 function to exclude potential outlier samples (see GitHub <https://github.com/privefl/bigutillsr>, and (23-
147 25)). These robust Mahalanobis distances are approximately Chi-square distributed, which enables
148 deriving p-values of outliers (Supplementary Table 2). Since we used 3 dimensions, we chose a p-value
149 threshold of 0.00111 (p-value < 0.01 with Bonferroni correction for multiple comparisons) which
150 concluded that patient 5 is an outlier in PCA2 & 3. This patient was removed from all downstream
151 analysis. Read counts of the 8 patients were normalized and tested for difference using DESeq2 (26).
152 Hierarchical clustering was carried out using Pearson correlation with complete linkage and on
153 differentially expressed genes (DEGs) which were filtered with the following parameters: baseMean >
154 5, padj < 0.1 and |logfoldchange| > 1. Pathway analysis was performed using Metascape, significant
155 pathways were determined if p < 0.05 and FDR < 0.5. STRING analysis was performed including all
156 DEGs.

157

158 **CAF isolation and RNA sequencing from *iLgr5;GLI2A* mice**

159 Gastric cancer was induced in *iLgr5;GLI2A* mice as described in (21). Gastric tumors were harvested
160 post mortem, washed, minced and dissociated using a gentleMACS dissociator and enzymatic
161 digestion with DMEM containing 3 mg ml⁻¹ collagenase A (#11088793001, Sigma Aldrich,) and 0.1
162 mg/ml Deoxyribonuclease I (#LS002007, Worthington) for 20 min at 37°C. The single cell suspension
163 was washed, filtered using 100 µm cell strainer, and immunostained. Normal gastric fibroblasts or
164 CAFs were collected based on negative selection for ghost dye, CD45, EpCAM, and CD31 and positive
165 selection for PDPN. RNA-seq was done by MARS-seq as described in (27). DEGs were filtered with
166 the following parameters: baseMean > 5, padj < 0.01 and |logfoldchange| > 3. Pathway analysis was
167 performed using Metascape, significant pathways were determined if p < 0.05 and FDR < 0.5.

168

169 **Validation of the patient and *iLgr5;GLI2A* mouse stromal signatures in independent patient**
170 **cohorts**

171 Patient data from the TCGA, Singapore (GSE15460), KUGH_KUCM (GSE26942), and ACRG
172 cohorts (GSE62254) were downloaded, individual gene values were transformed to z-scores and the
173 average of all known genes per sample was used to determine scores for the upregulated and
174 downregulated signatures. For the *INHBA-THBS1-THBS2* gene signature individual gene values were
175 transformed to z-scores and the average of genes per sample was determined. Gene symbols were
176 matched through Affymetrix Human Genome U133 Plus 2.0 Array or Illumina HumanHT-12 V4.0
177 expression bead chip. For patient cohorts GSE15460 and GSE62254 we could match 109 DEGs from
178 the CAF_up_sig and CAF_down_sig and for GSE26942 we could match 87 DEGs from the
179 CAF_up_sig and CAF_down_sig (out of the total 129 DEGs). For the *iLgr5;GLI2A* mCAF_up_sig
180 and mCAF_down_sig, 314 DEGs were matched in the GSE15460 and GSE62254 cohorts and 271
181 DEGs in the GSE26942 cohort (out of the total 361 DEGs). Median signature was calculated using
182 patients with complete survival and signature information. Kaplan Meier (KM) analysis of overall
183 survival with log rank p value was performed for each cancer type or patient cohort on patients
184 stratified by median expression of each of these signatures.

185

186 **HSF1 scoring and analysis**

187 Nuclear HSF1 staining in stroma and cancer cells of 72 patients was analysed by a trained pathologist
188 who was blinded to both patient outcome and clinical data. A scale of 0-3 (0-3: low ≤ 1 ; 1.5 <
189 intermediate ≤ 2 ; high >2) was set by the pathologist and scores were given based on nuclear staining
190 of HSF1 in stroma and cancer cells (Supplementary Table 1). Tissue samples were obtained from
191 surgical specimens. Patients diagnosed as stage 1-3 did not present with metastases at diagnosis. 8
192 patients diagnosed as stage 4 gastric cancer with metastases were omitted from further analysis. Overall
193 survival was defined as the time from first diagnosis to death based on the clinical data outlined in
194 Supplementary Table 1. The scores in cancer cells and CAFs showed different distributions. Therefore
195 for survival analysis of HSF1 activation in cancer cells, patients with low and intermediate scores were
196 combined and compared to patients with high scores, whereas for survival analysis of HSF1 activation
197 in CAFs, patients with high and intermediate scores were combined and compared to patients with low
198 scores (Supplementary Table 1). One patient could not be scored for cancer and for CAF HSF1 due to
199 insufficient tumor tissue and was therefore excluded from all statistical analyses. Two patients could
200 not be scored for CAF HSF1 and were excluded from CAF HSF1 analysis. Stage 2/3 was scored as
201 stage 2 in the final clinical analysis.

202

203 **Co-injection of recombinant Activin A and THBS2 with MC38 cancer cells into Nude mice**
204 MC38 (2×10^5) were incubated with either PBS, 2.5 μg of Activin A (#CYT -146, ProSpec), or 2.5 μg
205 of THBS2 (#1635-T2, R&D Systems) and co-injected in a total volume of 100 μl subcutaneously into
206 Nude mice (Harlan laboratories). 48h later a second dose of 2.5 μg recombinant protein was injected.
207 Tumors were measured by caliper for size and mice were sacrificed at day 15 due to high burden in the
208 Activin A group.

209

210 **Co-injection of EVs with MC38 cancer cells into Nude mice**

211 MC38 cells (2×10^5) were co-injected with either PBS or 1×10^{10} WT or *Hsfl* null EVs subcutaneously
212 into Nude mice (Harlan laboratories). 48h later a second dose (5×10^9) of EVs was injected. Tumors
213 were measured by caliper for size and the mice were sacrificed at day 17 due to high tumor burden.

214

215 **Data availability statement**

216 RNA sequencing data of *iLgr5;GLI2A* mice and patient samples were deposited in Gene Expression
217 Omnibus (GEO) and can be accessed via GSE162301 and GSE165211, respectively. All other data
218 supporting the findings of this study are available from the corresponding author on reasonable request.

219 **Results**

220 **CAFs express a transcriptional program that promotes malignancy and correlates with poor** 221 **disease outcome in gastric cancer**

222 Gastric CAFs have been attributed protumorigenic effects, however the genes contributing to these
223 effects are largely unknown. Therefore, we mapped the transcriptome of gastric CAFs in the
224 intratumoral stroma by laser capture microdissection (LCM) followed by RNA-sequencing
225 (Supplementary Fig. S1A). We isolated and sequenced CAF-rich stromal regions from formalin-fixed
226 paraffin-embedded (FFPE) tumor sections of 9 gastric cancer patients (Supplementary Fig. S1B-C and
227 Supplementary Table 1), representing favorable (survival) and poor prognostic (lethality) outcomes
228 (Supplementary Table 3). Principal component analysis (PCA) showed that stromal samples from these
229 patients clustered based on disease outcome (Fig. 1A and Supplementary Fig. S1D), while cancer
230 samples from the same patients did not (Fig. 1B and Supplementary Fig. S1E). Differential expression
231 analysis of stromal samples (see Materials and Methods, Supplementary Table 2 and Supplementary
232 Fig. S1F-G) revealed 129 differentially expressed genes (DEGs) between favorable and poor outcome
233 groups (Fig. 1C; Supplementary Table 3). ECM organization (involving genes such as *AEBP1*,
234 *COL10A1*, *COL11A1*, *SPOCK1*, *THBS2*, *EMILIN1*, and *TPM2*), response to growth factors (*INHBA*,

235 *FGFR1*, *HSPB1*) and mesenchymal cell proliferation (*LMNA*, *UACA*) were the most differentially
236 upregulated pathways in the stroma of patients with poor outcome (compared to patients with favorable
237 outcome; Fig. 1C and Supplementary Table 4). The humoral immune response (involving genes such
238 as *LCN2*, *PGC*, *REG1A*, *ITLNI*, *BPIFB1*, and *BIRC3*), digestive tract development (*GATA6*, *ITGA6*,
239 *CLDN18*), and tissue homeostasis (*LYZ*, *MUC6*) were most significantly downregulated in these
240 patients' stroma, compared to patients with favorable outcome (Fig. 1C and Supplementary Table 4).
241 Analysis of cancer samples from the same patients highlighted only 13 DEGs, and no significant
242 differentially regulated pathways (Supplementary Table 3 and Supplementary Fig. S1H).

243 The observed changes in stromal gene expression could be driven by differences in stromal abundance
244 between the patient groups. To test this, we performed image analysis to quantify stroma, cancer, and
245 immune regions in Hematoxylin Eosin (H&E) stained FFPE sections from the patients. We found no
246 significant difference in the percentage of stroma, cancer and immune cells between the favorable and
247 poor outcome patients, suggesting that it is not the abundance, but the transcriptional program that is
248 different between the two groups (Supplementary Fig. S1I-L). These findings suggest that as tumors
249 progress, stromal pathways involved in maintaining normal stomach functions are replaced by
250 pathways resulting from tumor-stroma interactions that support tumor growth.

251 We next set out to test the correlation between our stromal signature and clinical characteristics in
252 independent datasets. Since no pure gastric CAF datasets with reported disease outcome are available,
253 to the best of our knowledge, we turned to published datasets from bulk tumors and asked whether a
254 stromal signature comprised of genes upregulated in poor outcome patients in our dataset
255 (CAF_up_sig) could be detected in bulk tumors (including both stroma and cancer cells). First, we
256 analyzed The Cancer Genome Atlas (TCGA) datasets for gastro-intestinal (GI) tract cancers (gastric,
257 colorectal, pancreatic, hepatocellular, esophageal; Fig. 1D-E and Supplementary Table 5), and found
258 that the CAF_up_sig is significantly associated with poor outcome in gastric cancer and in colorectal
259 cancer (Fig. 1D-E). Genes downregulated in the stroma (CAF_down_sig) did not show any significant
260 association with survival (Supplementary Fig. S1M-N).

261 We then analyzed datasets from three other large patient cohorts: The Singapore cohort, the
262 KUGH_KUCM cohort, and the ACRG cohort (Supplementary Table 6). CAF_up_sig expression
263 significantly associated with poor overall survival in the Singapore cohort and in the KUGH_KUCM
264 cohort, and a similar trend was found with the ACRG cohort (Fig. 2A-C). Our CAF_down_sig showed
265 an opposite trend – high expression of CAF_down_sig significantly correlated with favorable outcome
266 in the Singapore and KUGH_KUCM cohorts, and a similar mild trend was observed with the ACRG
267 cohort (Fig. 2D-F). Univariate analysis showed that CAF_up_sig expression, cancer stage and presence

268 of metastasis were associated with poor overall survival in the Singapore and the KUGH_KUCM
269 cohorts and the ACRG cohort showed a similar trend (Supplementary Table 6).

270 We next looked for potential associations between expression of our CAF signature and gastric cancer
271 subtypes. In all 3 patient datasets, CAF_up_sig expression, but not CAF_down_sig expression, was
272 significantly enriched in the diffuse gastric cancer subtype, which typically has a worse prognosis
273 compared to the intestinal subtype (Fig. 2G-I and Supplementary Fig. S2A-C). In addition to the
274 histological classification of gastric cancer to diffuse and intestinal subtypes, two independent
275 molecular classification methods were recently described (4,5): A mesenchymal phenotype (MP)
276 characterized by high genomic integrity and associated with poor survival, and an epithelial phenotype
277 (EP) characterized by low genomic integrity and associated with favorable survival, were identified in
278 the KUGH_KUCM cohort (5); and 4 molecular subtypes (MSS TP53⁻, MSS TP53⁺, MSI, EMT) were
279 characterized in the ACRG cohort, of which the EMT subtype was associated with the worst outcome
280 (4). Analyzing the KUGH_KUCM cohort, we found that the CAF_up_sig was significantly enriched
281 in the MP class, and the CAF-down_sig was significantly enriched in the EP class (Fig. 2J). In the
282 ACRG cohort, the CAF_up_sig was significantly enriched in the EMT subtype while the
283 CAF_down_sig was significantly enriched in MSS TP53^{+/-} subtypes, associated with more favorable
284 outcomes (Fig. 2K).

285 Supporting this classification, gene set enrichment analysis (GSEA) using MSigDB (Hallmark gene
286 sets, see Supplementary Materials and Methods) on the full stromal RNA-seq dataset highlighted EMT
287 as the most significantly enriched pathway in patients with poor outcome compared to patients with
288 favorable outcome (Supplementary Fig. S2D and Supplementary Table 7). These analyses collectively
289 indicate that the stromal signature correlates with diffuse, mesenchymal and aggressive gastric cancer
290 subtypes, further reinforcing the clinical relevance of our stromal classification and pointing to specific
291 genes for dissection and targeting.

292

293 **A transcriptional signature derived from mouse PDPN⁺ gastric CAFs is associated with** 294 **aggressive gastric cancer phenotypes and poor disease outcome in patients**

295 To further dissect the contribution of CAFs to gastric cancer we induced gastric cancer in mice using
296 a triple-transgenic gastric cancer mouse model- *Lgr5-EGFP-IRES-CreERT2; R26-LSL-rtTA-IRES-*
297 *EGFP; tetO-GLI2A* mice, (*iLgr5;GLI2A* mice) (21). This model is based on deregulated activation of
298 the Hedgehog pathway by expression of GLI2A, an activated form of GLI2, in *Lgr5* expressing stem
299 cells in the stomach (21). We isolated CAFs and normal fibroblasts from the stomachs of gastric
300 cancer-induced and naïve *iLgr5;GLI2A* mice, and performed RNA-sequencing to obtain a pure mouse
301 CAF transcriptional signature (Supplementary Table 8). To that end tumors were excised 3 weeks after

302 GLI2A induction, and CAFs were isolated by fluorescence activated cell sorting (FACS) based on
303 negative selection for CD45 (immune), EpCAM (epithelial), and CD31 (endothelial cells), and positive
304 selection for PDPN (fibroblasts) (Supplementary Fig. S3A and Supplementary Table 9) (16,28,29).
305 154 genes were differentially upregulated and 207 were differentially downregulated in CAFs
306 compared to normal gastric fibroblasts (Supplementary Table 8). Pathway analysis highlighted similar
307 pathways to those discovered in the stromal dissection of the human patient samples: ECM
308 organization (*Adam12, Acan, Lox*), activation of matrix metalloproteinases (*Mmp3, Mmp9, Mmp10,*
309 *Mmp13*), response to growth factors (*Inhba, Grem1, Runx3*) and regulation of hormone levels (*Inhba,*
310 *Cnr1, Cpe*) were among the most differentially upregulated pathways in mouse CAFs, whereas
311 digestion (*Apoa1, Tff1, Pgc*) and tissue homeostasis (*Atp4a, Car2, Cldn18*) were the most differentially
312 downregulated pathways compared to normal gastric fibroblasts (Supplementary Table 10). We then
313 checked whether a signature comprised of genes upregulated in mouse CAFs (mCAF_up_sig) or genes
314 downregulated in mouse CAFs (mCAF_down_sig) would be associated with clinical characteristics in
315 the Singapore, KUGH_KUCM, and ACRG cohorts (Supplementary Table 11). Similar to the
316 CAF_up_sig from patient samples, high expression of the mCAF_up_sig significantly associated with
317 poor overall survival in the Singapore cohort and in the KUGH_KUCM cohort, and the ACRG cohort
318 showed a similar trend that was not statistically significant (Fig. 3A and Supplementary Fig. S3B-C).
319 The mCAF_down_sig showed an opposite trend- it was significantly associated with favorable
320 outcome in the Singapore cohort and a similar trend was seen in the KUGH_KUCM cohort (Fig. 3A
321 and Supplementary Fig. S3D). The ACRG cohort showed no particular trend for this analysis
322 (Supplementary Fig. S3E). The mCAF_up_sig also correlated with the more aggressive MP and EMT
323 molecular subtypes similar to the CAF_up signature from patient samples (Fig. 3B and Supplementary
324 Fig. S3F), whereas the mCAF_down_sig correlated with the less aggressive EP and MSS TP53^{+/-}
325 subtypes (Fig. 3B and Supplementary Fig. S3G). Collectively, the findings obtained from pure mouse
326 CAFs support our findings from patient samples, indicate that CAFs support gastric cancer and provide
327 potential targets and experimental systems for further characterization in mouse and human.

328 329 **INHBA and THBS1/2 are upregulated in gastric cancer stroma**

330 To characterize stromal pathways highlighted by our transcriptional profiling, we queried our patient
331 gene list for potential interactions of translated proteins using STRING (Fig. 3C). Based on this
332 analysis we chose to focus on two targets upregulated in poor outcome patients: inhibin Subunit Beta
333 A (INHBA) and thrombospondin 2 (THBS2), suggested to be part of a common signaling network
334 (30). Both targets were recently found by us to be highly expressed in a subset of wound-healing CAFs
335 in breast cancer (16). Moreover, they were both part of the EMT gene set highlighted by the GSEA

336 analysis as enriched in patients with poor outcome (Supplementary Fig. S2D and Supplementary Table
337 7). We added to this analysis thrombospondin 1 (THBS1), a close homologue of THBS2 that showed
338 a similar trend of expression (Supplementary Table 3) and was also included in the enriched EMT gene
339 set (Supplementary Table 7). *Inhba* was differentially upregulated also in mouse CAFs from
340 *iLgr5;GLI2A* tumors, and *Thbs1/2* showed a similar trend (Fig. 3D-F). INHBA is a subunit of Activin
341 and Inhibin, dimeric proteins belonging to the TGF β superfamily (31,32). Activin A is a homodimer
342 of two INHBA subunits, whereas Inhibin A and Activin AB are heterodimers of INHBA with INHA
343 and INHBB, respectively (32). INHBA is known to play a role in inflammation, tissue repair and
344 activation of myofibroblasts, and increased levels of INHBA are associated with lymph node (LN)
345 metastasis, gastric cancer cell proliferation and chemoresistance (33). THBS1/2 are adhesive
346 glycoproteins involved in cell-cell and cell-matrix interactions. Increased levels of THBS2 are
347 associated with LN metastasis and increased invasion in gastric cancer (34). The role of THBS1 is less
348 clear since it was implicated both in pro- and antitumorigenic activities in gastric cancer (35-37). Both
349 INHBA and THBS1/2 are known to play an important role in gastric cancer, however their role in the
350 TME is not well studied (30). To validate our RNA-seq results, we extracted total RNA from
351 *iLgr5;GLI2A* tumors and examined the levels of *Inhba*, *Thbs1* and *Thbs2* by qPCR. *Inhba* and *Thbs1*
352 levels were significantly upregulated in gastric tumors compared to normal gastric tissue and *Thbs2*
353 showed a similar trend (Fig. 3G-I). To define the tissue localization of INHBA and THBS1/2, and
354 confirm their expression at the protein level we performed immunohistochemistry (IHC) staining of
355 sections from *iLgr5;GLI2A* tumors and from normal stomach controls using antibodies against INHBA
356 and THBS1. INHBA and THBS1 were expressed at very low levels in normal gastric glands and
357 muscle (Fig. 3J-K). Gastric tumors however exhibited high levels of INHBA and THBS1 both in
358 stroma and in cancer cells (Fig. 3J-K). Together, these findings support our patient RNA-seq results
359 and suggest that INHBA and THBS1/2 are upregulated in gastric cancer stroma.

360 Given their connectivity to other genes in the stromal network revealed by the STRING analysis (Fig.
361 3C), and the potential simplicity of a 3-gene signature (compared to a signature comprised of dozens
362 of genes) we tested whether a minimal gene signature comprised of only *INHBA* and *THBS1/2* would
363 correlate with disease outcome in our patient datasets. We found that the 3-gene signature
364 (*INHBA/THBS1/THBS2*) correlated with poor disease outcome in the TCGA gastric cancer and
365 colorectal cancer datasets, the Singapore cohort and the KUGH_KUCM cohort (Supplementary Fig.
366 S4A-D and Supplementary Table 6). As with the other stromal signatures that we analyzed, the ACRG
367 cohort showed a similar trend of disease outcome that was not statistically significant (Supplementary
368 Fig. S4E), possibly due to differences in patient follow up time or cohort characteristics

369 (Supplementary Table 6). These results imply that stromal INHBA and THBS1/2 are associated with
370 aggressive disease phenotypes in gastric cancer, and serve as attractive targets for characterization.

371

372 **HSF1 activation in gastric CAFs is associated with poor disease outcome**

373 In search for potential transcriptional regulators of the stromal signature in general, and INHBA and
374 THBS1/2 in particular, we examined heat-shock factor 1 (HSF1). Previously we and others have shown
375 that HSF1, the master transcriptional regulator of the heat shock response, plays an important role in
376 the conversion of fibroblasts into CAFs in the TME (20,38). Moreover, *INHBA* and *THBS1* were
377 shown to be transcriptional targets of HSF1 (39,40). In gastric cancer, activation of HSF1 in cancer
378 cells was shown to correlate with poor disease outcome (41), yet the contribution of stromal HSF1 to
379 disease outcome has not been assessed. HSF1 translocates from the cytoplasm to the nucleus and binds
380 to heat shock elements in the DNA upon activation (39). Therefore, its nuclear localization is
381 commonly used as a proxy for HSF1 activation (39). Indeed, IHC staining of FFPE sections from
382 gastric cancer patients revealed nuclear HSF1 staining both in cancer cells and in CAFs, while normal
383 stomach glands and muscle exhibited low or no HSF1 staining (Fig. 4A).

384 To systematically test whether stromal activation of HSF1 is associated with disease outcome in gastric
385 cancer, we performed IHC staining for HSF1 and scored its nuclear localization in cancer cells and
386 CAFs, in sections from 64 gastric cancer patients (including the sub-cohort of LCM-RNA-seq patients)
387 with documented clinical characteristics and patient outcome data (Supplementary Table 1). High
388 HSF1 activation in cancer cells correlated with shorter overall survival time and stromal HSF1 showed
389 a similar trend (Fig. 4B-C and Supplementary Table 12). In the cohort of patients analyzed by LCM
390 and RNA-seq, all patients with poor outcomes also exhibited intermediate or high HSF1 activation (i.e.
391 nuclear localization) in cancer and stromal cells, while patients with favorable outcomes differed in
392 their HSF1 activation status (Supplementary Table 1). Interestingly, stromal HSF1 activation also
393 significantly correlated with HER2 status – HER2⁻ patients exhibited high HSF1 levels whereas HER2⁺
394 patients had low stromal HSF1 activation levels (Supplementary Table 1). These results imply that in
395 addition to its previously described roles in gastric cancer cells, HSF1 activates complementary
396 pathways in gastric stroma that promote aggressive disease phenotypes. This conclusion was further
397 supported by a multivariate Cox proportional-hazards regression analysis (Supplementary Table 12).
398 In an additive multivariate model considering tumor stage and HSF1 score, stromal HSF1 score and
399 tumor stage were significantly associated with overall survival (p=0.006), and this association was
400 more significant than that of cancer HSF1 and tumor stage with survival (p=0.016).

401

402 **Stromal INHBA and THBS1/2 are targets of HSF1, *in vitro***

403 Multiplexed immunofluorescent staining (MxIF) of gastric cancer patient samples showed that HSF1
404 is co-expressed with INHBA and THBS1, in cancer cells and in CAFs, while normal stomach tissue
405 exhibited low INHBA, THBS1 and HSF1 staining (Fig. 4D). To test whether HSF1 regulates INHBA
406 and THBS1/2 stromal expression, and whether this regulation affects cancer cells, we measured the
407 expression of INHBA and THBS1/2 in WT vs *Hsf1* null mouse embryonic fibroblasts (MEFs).
408 THBS1/2 and INHBA protein levels were significantly higher in WT MEFs compared to *Hsf1* null
409 MEFs (Fig. 5A-E). Next, we asked if INHBA and THBS1/2 expression in fibroblasts is affected by
410 co-culture with cancer cells. 72h of co-culture with N87 human gastric cancer cells led to a significant
411 increase in *Inhba*, *Thbs1* and *Thbs2* mRNA levels compared to cells grown in mono-culture (Fig. 5F-
412 H). Some induction was also observed in *Hsf1* null MEFs upon co-culture, however the total levels
413 were lower in *Hsf1* null MEFs compared to WT MEFs (Fig. 5F-H).

414 To determine how this stromal network affects cancer cells, we monitored cancer cell growth in co-
415 culture. N87 cells showed a significant growth reduction when co-cultured with *Hsf1* null MEFs
416 compared to WT MEFs (Fig. 5I-K), and similar results were observed upon co-culture of N87 cells
417 with human foreskin fibroblasts (HFFs) in which HSF1 was knocked down by siRNA (Fig. 5L and
418 Supplementary Fig. S5A-C).

419 Next we knocked down *INHBA*, *THBS1* and *THBS2* in fibroblasts and monitored gastric cancer cell
420 growth in co-culture. Knock down of *THBS2* in HFFs led to a minor decrease in N87 cell proliferation,
421 and knockdown of *THBS1* led to a minor increase in N87 proliferation (Supplementary Fig. S5D-F).
422 Knock down of *INHBA* however led to a substantial and significant decrease in the growth of co-
423 cultured N87 cells (Fig. 5M and Supplementary Fig. S5G). A combined knockdown of *HSF1*-*INHBA*-
424 *THBS2* had a similar effect on N87 growth (Fig. 5N), whereas the combination of *HSF1* and *INHBA*
425 with *THBS1* had a milder effect (Supplementary Fig. S5H). Collectively these results support the
426 hypothesis that HSF1, INHBA and THBS1/2 are part of a common stromal protumorigenic signaling
427 network, in which HSF1 regulates the expression of *THBS1/2* and *INHBA*. While INHBA and THBS2
428 seem to play a protumorigenic role in fibroblasts, THBS1 may be antitumorigenic.

429

430 **THBS2 and INHBA are secreted from fibroblasts via EVs, in an HSF1-dependent manner**

431 INHBA and THBS1/2 are secreted proteins (42). We therefore hypothesized that INHBA and THBS2
432 are secreted from CAFs to the TME where they act on cancer cells, and that this process could be
433 mimicked by exogenous treatment with recombinant proteins. To test this, we co-injected MC38 colon
434 cancer cells with recombinant proteins into mice, subcutaneously, followed by another injection of
435 recombinant protein two days later, and monitored tumor growth. Co-injection of either THBS2 or
436 Activin A (a homodimer of two INHBA subunits (31)) with MC38 cancer cells significantly increased

437 the tumorigenicity of these cells – larger and faster growing tumors formed in the presence of THBS2
438 or Activin A (Fig. 6A).

439 INHBA and THBS1/2 have been proposed to shuttle through EVs (43-49). Recently, THBS2 was
440 shown to be a marker for exosomes secreted by tumors (50). We therefore hypothesized that the
441 protumorigenic effects of stromal HSF1 may be mediated by secretion and delivery of these proteins
442 to the TME, possibly via EVs. Small EVs are lipid bilayer-enclosed particles sized 30-150 nm, that
443 mediate cell-cell communication via targeting, fusion and release of content from one cell to another
444 (51). Their cargo includes bioactive molecules such as effector proteins, metabolites, large and small
445 RNAs and even genomic DNA (50). Recently, EVs secreted from stromal cells were shown to
446 contribute to disease progression and poor disease outcome by promoting vascularization and
447 chemotherapy resistance (52). To test whether INHBA and THBS1/2 are secreted via EVs in an HSF1-
448 dependent manner, we first confirmed the presence of INHBA and THBS1/2 in EVs by OptiPrep
449 density gradient isolation of EVs secreted from WT MEFs (Fig. 6B-C and Supplementary Fig. S6A).
450 ALIX and TSG101, two known exosome markers, were used as positive loading controls (53). HSF1
451 is not expected to be found in EVs and therefore served as a negative control. ALIX and TSG101 were
452 found in fractions 3-8. Both proteins peaked in high density fractions (6-7), and TSG101 had an
453 additional peak in low density fraction 4 (Fig. 6B-C). HSF1 was not detected in any of these fractions.
454 INHBA and THBS1/2, however, were detected in fractions 2-7, and peaked in fractions 4-5 (Fig. 6B-
455 C). To confirm that these fractions contain EVs we performed transmission electron microscope
456 (TEM) analysis. We found that EVs are indeed observed in both low- and high-density fractions (Fig.
457 6D). These observations suggest that two populations of EVs are secreted by MEFs – a low density
458 population, enriched in INHBA and THBS1/2 (Supplementary Fig. S6A) and a high-density
459 population with lower levels of INHBA and THBS1/2. We also checked the presence of INHBA and
460 THBS1/2 in EVs isolated from the serum of *iLgr5;GLI2A* mice. While we could not detect THBS1/2
461 in the serum (possibly due to low sensitivity of the assay), INHBA was detected, and its levels were
462 significantly higher in EVs isolated from the serum of tumor-bearing *iLgr5;GLI2A* mice compared to
463 EVs isolated from the serum of naïve *iLgr5;GLI2A* mice (Fig. 6E-F).

464 We then compared the expression levels of INHBA and THBS1/2 in EVs isolated from WT *vs Hsfl*
465 null fibroblasts. While THBS1 levels were similar between WT and *Hsfl* null-derived EVs, THBS2
466 and INHBA levels were significantly higher in EVs derived from WT MEFs compared to EVs from
467 *Hsfl* null MEFs (Fig. 6G-J). These results suggest that INHBA and THBS2 expression in EVs is HSF1-
468 dependent.

469 To examine whether the differential expression of INHBA and THBS2 was due to impaired EV
470 biogenesis in *Hsfl* null MEFs, we compared the number and size of EVs produced by each genotype

471 using nanoparticle tracking analysis (NTA). We could not detect differences in size or in quantity
472 between EVs secreted from WT and *Hsf1* null fibroblasts (Supplementary Fig. S6B-E). We extended
473 our analysis to field-flow fractionation (FFF), to better separate EV populations and assess smaller EV
474 populations shown to be biologically active (54). Similar to our NTA analysis, FFF did not detect
475 consistent differences between EVs derived from *Hsf1* null MEFs compared to WT MEFs
476 (Supplementary Fig. S6F). We next tested whether the differences in protein content could be due to
477 impaired uptake of EVs derived from *Hsf1* null compared to WT MEFs. We incubated N87 gastric
478 cancer cells and MC38 colon cancer cells with CFSE stained EVs, and analyzed uptake 12-16h later
479 by imaging the cells in an ImageStream imaging flow cytometer. We could not detect differences in
480 the percentage of CFSE⁺ N87 and MC38 cells incubated in the presence of EVs from *Hsf1* null
481 compared to WT MEFs (Supplementary Fig. S6G-O), indicating that HSF1 does not affect EV
482 biogenesis or uptake, yet it plays an important role in the protein content of EVs.

483 To assess the biological relevance of these findings we co-injected EVs derived from WT vs *Hsf1* null
484 MEFs together with MC38 cancer cells into nude mice, and monitored tumor growth. Co-injection
485 with EVs derived from WT MEFs caused a significant increase in the growth of MC38-injected tumors
486 (Fig. 6K). This effect was completely abolished when EVs from *Hsf1* null MEFs were co-injected with
487 MC38 cells. Taken together these experiments show that EVs derived from WT and *Hsf1* null MEFs
488 are similar in size, quantity, biogenesis and uptake into cancer cells. However, there is a significant
489 difference in their content and, consequently, their effect on tumor growth. These findings imply that
490 HSF1 regulates the expression of INHBA and THBS1/2 in stromal cells. INHBA and THBS2 are then
491 packaged into EVs in an HSF1-dependent manner and secreted to the TME, where they are taken up
492 by cancer cells and promote a more aggressive disease phenotype (Fig. 6L).

493

494 **Discussion**

495 Despite recent advances in molecular subtyping, the backbone of gastric cancer treatment remains
496 chemotherapeutic combinations. Molecular classifications, based largely on mutations and genomic
497 alterations in the cancer cells, do not translate to guide treatment modality. Here we chose a
498 complementary approach - searching for transcriptional changes in the gastric TME. We defined a
499 stromal gene signature associated with poor disease outcome in patients, and found a role for the
500 stromal master transcriptional regulator HSF1 in driving it, through exosome-mediated secretion of
501 protumorigenic proteins that are taken up by cancer cells to promote aggressive disease phenotypes.
502 HSF1 was previously shown by us and others to play protumorigenic roles in CAFs of breast, lung and
503 colon carcinomas (17,20,38). The finding that HSF1 also acts in gastric CAFs implicates HSF1 as a
504 master regulator of CAF activities in carcinomas across different tissues, and suggests that its

505 protumorigenic effects - in gastric cancer and other carcinomas - may be mediated via delivery of
506 targets to the TME in EVs.

507 INHBA and THBS1/2 are involved in tumor progression and were shown to be co-regulated (30,55,56)
508 possibly sharing common signaling pathways. While INHBA and THBS2 are protumorigenic, THBS1
509 was proposed to exert both pro and antitumorigenic effects, depending on the system examined
510 (44,55,57). Our findings suggest that all 3 proteins are upregulated in CAFs in an HSF1-dependent
511 manner. Our *in vitro* experiments and mouse co-injections with recombinant proteins show a clear
512 protumorigenic role of Activin A and THBS2, while the effect of stromal THBS1 on cancer cells (*in*
513 *vitro*) is less clear. Taken together with the finding that INHBA and THBS2 are delivered into
514 exosomes in an HSF1-dependent manner, while THBS1 exosomal expression is not affected by HSF1
515 status, it is possible that selective delivery of INHBA and THBS2 to exosomes leads to the
516 protumorigenic effect observed, while THBS1 is antitumorigenic.

517 EV cargo includes proteins, metabolites, RNA and genomic DNA (50), which could serve as bioactive
518 molecules in the TME. In GI-tract cancers, EVs from CAFs were shown to promote cancer through
519 delivery of miRNAs to gastric cancer cells to suppress ferroptosis (58), and Wnt glycoproteins to
520 colorectal cancer cells to induce cancer stemness and chemoresistance (59). In our study, differential
521 protein expression in EVs affects their activity. Though biogenesis and uptake of EVs was not
522 impaired, loss of HSF1 abolished the protumorigenic effect of EVs derived from WT MEFs. Our
523 findings indicate that EV cargo is selective and the content is affected by HSF1.

524 Over the last years, efforts were made to identify gastric cancer drivers and gene signatures that may
525 serve as biomarkers for diagnosis and treatment (3). Trastuzumab revolutionized the treatment of
526 HER2-positive gastric cancers (60), and immunotherapy has proven to be an effective therapy for
527 patients with microsatellite instability (MSI) (61). Other signatures, such as those associated with
528 *Helicobacter pylori* and *EBV* infections (62,63), germline mutations of *CDHI*, mismatch repair genes
529 (64,65), epithelial vs mesenchymal cell types (5), and MSS TP53⁻, MSS TP53⁺, MSI, EMT subtypes
530 (4) enabled associations between molecular landscape and gastric cancer subtyping (3,60). However,
531 the TME of gastric cancer in general, and the molecular composition of gastric CAFs in particular,
532 have been scarcely studied. Our profiling of CAFs from patient tumors highlights stromal compositions
533 associated with the aggressive diffuse and EMT-like gastric cancer subtypes. These targets should be
534 further explored, certainly as prognostic targets and hopefully as robust therapeutic targets in gastric
535 cancer.

536

537 **Acknowledgments**

538 Mouse pathological evaluation was carried out by Ori Brenner (WIS). Bioinformatic analyses were
539 assisted by Ester Feldmesser, Ron Rotkopf, and Irit Orr (WIS). We thank Raya Eilam-Altstadter for
540 assistance with immunostaining, Andreas Moor for guidance with LCM, Rawand Hamodi for technical
541 assistance and members of the Scherz-Shouval lab for their valuable input. R.S.S. is supported by ISF
542 grants 401/17 and 1384/1, ERC grant 754320, the Israel cancer research fund, the Abisch-Frenkel
543 foundation, the Laura Gurwin Flug Family Fund, the Peter and Patricia Gruber Awards, the Comisaroff
544 Family Trust, the Estate of Annice Anzelewitz, and the Estate of Mordecai M. Roshwal. R.S.S. is the
545 incumbent of the Ernst and Kaethe Ascher Career Development Chair in Life Sciences. A.A.D. was
546 supported by NIH grants R01 CA118875 and P30 CA046592.

547

548

549

550 References

- 551 1. Corso S, Isella C, Bellomo SE, Apicella M, Durando S, Migliore C, *et al.* A Comprehensive PDX Gastric
552 Cancer Collection Captures Cancer Cell-Intrinsic Transcriptional MSI Traits. *Cancer Res* **2019**;79:5884-96
553 2. Lordick F, Allum W, Carneiro F, Mitry E, Tabernero J, Tan P, *et al.* Unmet needs and challenges in gastric
554 cancer: the way forward. *Cancer Treat Rev* **2014**;40:692-700
555 3. Cancer Genome Atlas Research N. Comprehensive molecular characterization of gastric adenocarcinoma.
556 *Nature* **2014**;513:202-9
557 4. Cristescu R, Lee J, Nebozhyn M, Kim KM, Ting JC, Wong SS, *et al.* Molecular analysis of gastric cancer
558 identifies subtypes associated with distinct clinical outcomes. *Nat Med* **2015**;21:449-56
559 5. Oh SC, Sohn BH, Cheong JH, Kim SB, Lee JE, Park KC, *et al.* Clinical and genomic landscape of gastric cancer
560 with a mesenchymal phenotype. *Nature Communications* **2018**;9
561 6. Tan IB, Ivanova T, Lim KH, Ong CW, Deng NT, Lee J, *et al.* Intrinsic Subtypes of Gastric Cancer, Based on
562 Gene Expression Pattern, Predict Survival and Respond Differently to Chemotherapy. *Gastroenterology*
563 **2011**;141:476-U551
564 7. Van Cutsem E, Sagaert X, Topal B, Haustermans K, Prenen H. Gastric cancer. *Lancet* **2016**;388:2654-64
565 8. Becker KF, Keller G, Hoefler H. The use of molecular biology in diagnosis and prognosis of gastric cancer.
566 *Surg Oncol* **2000**;9:5-11
567 9. Tabassum DP, Polyak K. Tumorigenesis: it takes a village. *Nat Rev Cancer* **2015**;15:473-83
568 10. Hanahan D, Coussens LM. Accessories to the Crime: Functions of Cells Recruited to the Tumor
569 Microenvironment. *Cancer Cell* **2012**;21:309-22
570 11. Morihito T, Kuroda S, Kanaya N, Kakiuchi Y, Kubota T, Aoyama K, *et al.* PD-L1 expression combined with
571 microsatellite instability/CD8+ tumor infiltrating lymphocytes as a useful prognostic biomarker in gastric
572 cancer. *Sci Rep* **2019**;9:4633
573 12. Sahai E, Astsaturov I, Cukierman E, DeNardo DG, Egeblad M, Evans RM, *et al.* A framework for advancing
574 our understanding of cancer-associated fibroblasts. *Nat Rev Cancer* **2020**;20:174-86
575 13. Erez N, Truitt M, Olson P, Arron ST, Hanahan D. Cancer-Associated Fibroblasts Are Activated in Incipient
576 Neoplasia to Orchestrate Tumor-Promoting Inflammation in an NF-kappa B-Dependent Manner (vol 17, pg 135,
577 2010). *Cancer Cell* **2010**;17:523-
578 14. Finak G, Bertos N, Pepin F, Sadkova S, Souleimanova M, Zhao H, *et al.* Stromal gene expression predicts
579 clinical outcome in breast cancer. *Nat Med* **2008**;14:518-27
580 15. Kalluri R. The biology and function of fibroblasts in cancer. *Nat Rev Cancer* **2016**;16:582-98
581 16. Friedman G, Levi-Galibov O, David E, Bornstein C, Giladi A, Dadiani M, *et al.* Cancer-associated fibroblast
582 compositions change with breast-cancer progression linking S100A4 and PDPN ratios with clinical outcome.
583 *Nature Cancer* **2020**
584 17. Levi-Galibov O, Lavon, H., Wassermann-Dozorets, R. *et al.* Heat Shock Factor 1-dependent extracellular matrix
585 remodeling mediates the transition from chronic intestinal inflammation to colon cancer. *Nature*
586 *Communications* **2020**

- 587 18. Zhi KK, Shen XJ, Zhang H, Bi JW. Cancer-associated fibroblasts are positively correlated with metastatic
588 potential of human gastric cancers. *J Exp Clin Canc Res* **2010**;29
- 589 19. Li BL, Jiang YM, Li GX, Fisher GA, Li RJ. Natural killer cell and stroma abundance are independently
590 prognostic and predict gastric cancer chemotherapy benefit. *Jci Insight* **2020**;5
- 591 20. Scherz-Shouval R, Santagata S, Mendillo ML, Sholl LM, Ben-Aharon I, Beck AH, *et al.* The reprogramming of
592 tumor stroma by HSF1 is a potent enabler of malignancy. *Cell* **2014**;158:564-78
- 593 21. Syu LJ, Zhao X, Zhang Y, Grachtchouk M, Demitrack E, Ermilov A, *et al.* Invasive mouse gastric
594 adenocarcinomas arising from Lgr5⁺ stem cells are dependent on crosstalk between the Hedgehog/GLI2 and
595 mTOR pathways. *Oncotarget* **2016**;7:10255-70
- 596 22. McMillan DR, Xiao XZ, Shao L, Graves K, Benjamin IJ. Targeted disruption of heat shock transcription factor
597 1 abolishes thermotolerance and protection against heat-inducible apoptosis. *J Biol Chem* **1998**;273:7523-8
- 598 23. Yohai VJ, Zamar RH. High Breakdown-Point Estimates of Regression by Means of the Minimization of an
599 Efficient Scale. *J Am Stat Assoc* **1988**;83:406-13
- 600 24. Maronna RA, Zamar RH. Robust estimates of location and dispersion for high-dimensional datasets.
601 *Technometrics* **2002**;44:307-17
- 602 25. Gnanadesikan R, Kettenring JR. Robust Estimates, Residuals, and Outlier Detection with Multiresponse Data.
603 *Biometrics* **1972**;28:81-+
- 604 26. Love MI, Huber W, Anders S. Moderated estimation of fold change and dispersion for RNA-seq data with
605 DESeq2. *Genome Biol* **2014**;15:550
- 606 27. Jaitin DA, Kenigsberg E, Keren-Shaul H, Elefant N, Paul F, Zaretsky I, *et al.* Massively Parallel Single-Cell
607 RNA-Seq for Marker-Free Decomposition of Tissues into Cell Types. *Science* **2014**;343:776-9
- 608 28. Maruyama S, Furuya S, Shiraishi K, Shimizu H, Akaike H, Hosomura N, *et al.* Podoplanin Expression as a
609 Prognostic Factor in Gastric Cancer. *Anticancer Res* **2018**;38:2717-22
- 610 29. Shindo K, Aishima S, Ohuchida K, Fujiwara K, Fujino M, Mizuuchi Y, *et al.* Podoplanin expression in cancer-
611 associated fibroblasts enhances tumor progression of invasive ductal carcinoma of the pancreas. *Molecular*
612 *Cancer* **2013**;12
- 613 30. Kim H, Watkinson J, Varadan V, Anastassiou D. Multi-cancer computational analysis reveals invasion-
614 associated variant of desmoplastic reaction involving INHBA, THBS2 and COL11A1. *BMC Med Genomics*
615 **2010**;3:51
- 616 31. Link AS, Zheng F, Alzheimer C. Activin Signaling in the Pathogenesis and Therapy of Neuropsychiatric
617 Diseases. *Front Mol Neurosci* **2016**;7
- 618 32. Namwanje M, Brown CW. Activins and Inhibins: Roles in Development, Physiology, and Disease. *Cold Spring*
619 *Harb Perspect Biol* **2016**;8
- 620 33. Seeruttun SR, Cheung WY, Wang W, Fang C, Liu ZM, Li JQ, *et al.* Identification of molecular biomarkers for
621 the diagnosis of gastric cancer and lymph-node metastasis. *Gastroenterol Rep (Oxf)* **2019**;7:57-66
- 622 34. Oue N, Aung PP, Mitani Y, Kuniyasu H, Nakayama H, Yasui W. Genes involved in invasion and metastasis of
623 gastric cancer identified by array-based hybridization and serial analysis of gene expression. *Oncology* **2005**;69
624 Suppl 1:17-22
- 625 35. Hong BB, Chen SQ, Qi YL, Zhu JW, Lin JY. Association of THBS1 rs1478605 T>C in 5'-untranslated regions
626 with the development and progression of gastric cancer. *Biomed Rep* **2015**;3:207-14
- 627 36. Huang T, Wang L, Liu D, Li P, Xiong H, Zhuang L, *et al.* FGF7/FGFR2 signal promotes invasion and migration
628 in human gastric cancer through upregulation of thrombospondin-1. *Int J Oncol* **2017**;50:1501-12
- 629 37. Sun C, Yuan Q, Wu D, Meng X, Wang B. Identification of core genes and outcome in gastric cancer using
630 bioinformatics analysis. *Oncotarget* **2017**;8:70271-80
- 631 38. Ferrari N, Ranftl R, Chicherova I, Slaven ND, Moeendarbary E, Farrugia AJ, *et al.* Dickkopf-3 links HSF1 and
632 YAP/TAZ signalling to control aggressive behaviours in cancer-associated fibroblasts. *Nat Commun*
633 **2019**;10:130
- 634 39. Mendillo ML, Santagata S, Koeva M, Bell GW, Hu R, Tamimi RM, *et al.* HSF1 drives a transcriptional program
635 distinct from heat shock to support highly malignant human cancers. *Cell* **2012**;150:549-62
- 636 40. Kovacs D, Sigmond T, Hotzi B, Bohar B, Fazekas D, Deak V, *et al.* HSF1Base: A Comprehensive Database of
637 HSF1 (Heat Shock Factor 1) Target Genes. *Int J Mol Sci* **2019**;20
- 638 41. Dai W, Ye J, Zhang Z, Yang L, Ren H, Wu H, *et al.* Increased expression of heat shock factor 1 (HSF1) is
639 associated with poor survival in gastric cancer patients. *Diagn Pathol* **2018**;13:80
- 640 42. Uhlen M, Fagerberg L, Hallstrom BM, Lindskog C, Oksvold P, Mardinoglu A, *et al.* Proteomics. Tissue-based
641 map of the human proteome. *Science* **2015**;347:1260419
- 642 43. Becker A, Thakur BK, Weiss JM, Kim HS, Peinado H, Lyden D. Extracellular Vesicles in Cancer: Cell-to-Cell
643 Mediators of Metastasis. *Cancer Cell* **2016**;30:836-48
- 644 44. Huang WT, Chong IW, Chen HL, Li CY, Hsieh CC, Kuo HF, *et al.* Pigment epithelium-derived factor inhibits
645 lung cancer migration and invasion by upregulating exosomal thrombospondin 1. *Cancer Lett* **2019**;442:287-98

- 646 45. Morhayim J, van de Peppel J, Demmers JA, Kocer G, Nigg AL, van Driel M, *et al.* Proteomic signatures of
647 extracellular vesicles secreted by nonmineralizing and mineralizing human osteoblasts and stimulation of tumor
648 cell growth. *FASEB J* **2015**;29:274-85
- 649 46. Sobral LM, Bufalino A, Lopes MA, Graner E, Salo T, Coletta RD. Myofibroblasts in the stroma of oral cancer
650 promote tumorigenesis via secretion of activin A. *Oral Oncol* **2011**;47:840-6
- 651 47. Stenina OI, Topol EJ, Plow EF. Thrombospondins, their polymorphisms, and cardiovascular disease.
652 *Arterioscler Thromb Vasc Biol* **2007**;27:1886-94
- 653 48. Xiao M, Zhang J, Chen W, Chen W. M1-like tumor-associated macrophages activated by exosome-transferred
654 THBS1 promote malignant migration in oral squamous cell carcinoma. *J Exp Clin Cancer Res* **2018**;37:143
- 655 49. Zhang XW, Zhou JC, Peng D, Hua F, Li K, Yu JJ, *et al.* Disrupting the TRIB3-SQSTM1 interaction reduces
656 liver fibrosis by restoring autophagy and suppressing exosome-mediated HSC activation. *Autophagy*
657 **2020**;16:782-96
- 658 50. Hoshino A, Kim HS, Bojmar L, Gyan KE, Cioffi M, Hernandez J, *et al.* Extracellular Vesicle and Particle
659 Biomarkers Define Multiple Human Cancers. *Cell* **2020**;182:1044-61 e18
- 660 51. van Niel G, D'Angelo G, Raposo G. Shedding light on the cell biology of extracellular vesicles. *Nat Rev Mol*
661 *Cell Biol* **2018**;19:213-28
- 662 52. Boelens MC, Wu TJ, Nabet BY, Xu B, Qiu Y, Yoon T, *et al.* Exosome transfer from stromal to breast cancer
663 cells regulates therapy resistance pathways. *Cell* **2014**;159:499-513
- 664 53. Willms E, Johansson HJ, Mager I, Lee Y, Blomberg KE, Sadik M, *et al.* Cells release subpopulations of
665 exosomes with distinct molecular and biological properties. *Sci Rep* **2016**;6:22519
- 666 54. Zhang H, Freitas D, Kim HS, Fabijanic K, Li Z, Chen H, *et al.* Identification of distinct nanoparticles and
667 subsets of extracellular vesicles by asymmetric flow field-flow fractionation. *Nat Cell Biol* **2018**;20:332-43
- 668 55. Wang X, Zhang L, Li H, Sun WJ, Zhang HH, Lai MD. THBS2 is a Potential Prognostic Biomarker in Colorectal
669 Cancer. *Sci Rep-Uk* **2016**;6
- 670 56. Weng TY, Wang CY, Hung YH, Chen WC, Chen YL, Lai MD. Differential Expression Pattern of THBS1 and
671 THBS2 in Lung Cancer: Clinical Outcome and a Systematic-Analysis of Microarray Databases. *Plos One*
672 **2016**;11
- 673 57. Kashihara H, Shimada M, Yoshikawa K, Higashijima J, Tokunaga T, Nishi M, *et al.* Correlation Between
674 Thrombospondin-1 Expression in Non-cancer Tissue and Gastric Carcinogenesis. *Anticancer Res* **2017**;37:3547-
675 52
- 676 58. Zhang H, Deng T, Liu R, Ning T, Yang H, Liu D, *et al.* CAF secreted miR-522 suppresses ferroptosis and
677 promotes acquired chemo-resistance in gastric cancer. *Mol Cancer* **2020**;19:43
- 678 59. Hu YB, Yan C, Mu L, Mi YL, Zhao H, Hu H, *et al.* Exosomal Wnt-induced dedifferentiation of colorectal
679 cancer cells contributes to chemotherapy resistance. *Oncogene* **2019**;38:1951-65
- 680 60. Gunturu KS, Woo Y, Beaubier N, Remotti HE, Saif MW. Gastric cancer and trastuzumab: first biologic therapy
681 in gastric cancer. *Ther Adv Med Oncol* **2013**;5:143-51
- 682 61. Yuza K, Nagahashi M, Watanabe S, Takabe K, Wakai T. Hypermutation and microsatellite instability in
683 gastrointestinal cancers. *Oncotarget* **2017**;8:112103-15
- 684 62. Uemura N, Okamoto S, Yamamoto S, Matsumura N, Yamaguchi S, Yamakido M, *et al.* Helicobacter pylori
685 infection and the development of gastric cancer. *N Engl J Med* **2001**;345:784-9
- 686 63. Zhao Y, Zhang J, Cheng ASL, Yu J, To KF, Kang W. Gastric cancer: genome damaged by bugs. *Oncogene*
687 **2020**;39:3427-42
- 688 64. Keller G, Grimm V, Vogelsang H, Bischoff P, Mueller J, Siewert JR, *et al.* Analysis for microsatellite instability
689 and mutations of the DNA mismatch repair gene hMLH1 in familial gastric cancer. *Int J Cancer* **1996**;68:571-6
- 690 65. Richards FM, McKee SA, Rajpar MH, Cole TR, Evans DG, Jankowski JA, *et al.* Germline E-cadherin gene
691 (CDH1) mutations predispose to familial gastric cancer and colorectal cancer. *Hum Mol Genet* **1999**;8:607-10

692

693 **Figure Legends**

694 **Fig 1. The transcriptional landscape of gastric cancer stroma changes with disease**
695 **aggressiveness.** CAF-rich or cancer-rich regions of tumor sections from 9 gastric cancer patients were
696 laser-capture microdissected and analyzed by RNA-sequencing. Principal component analysis (PCA)
697 was performed for (A) CAFs and (B) cancer cells. Purple/orange dots - survival/lethality, as indicated.
698 (C) Heatmap showing hierarchical clustering of 129 genes differentially expressed in CAF-rich
699 samples with favorable vs poor outcome. Pathway analysis was performed using Metascape. Selected
700 significant pathways ($p < 0.05$, FDR < 0.5) are shown (see Supplementary Table 4). Purple/orange
701

702 bars - survival/lethality, as indicated. **(D-E)** Kaplan-Meier (KM) analysis showing overall survival of
703 **(D)** gastric or **(E)** colorectal cancer patients from the TCGA stratified based on median expression of
704 the stromal gene signature (CAF_up_sig).

705 **Fig 2. High expression of the CAF signature is associated with aggressive disease and poor**
706 **disease outcome in gastric cancer patients. (A-C)** KM analysis showing overall survival of patients
707 from **(A)** the Singapore cohort; **(B)** the KUGH & KUCM cohort; and **(C)** the ACRG cohort stratified
708 based on expression of the upregulated (CAF_up_sig) stromal gene signature. **(D-F)** KM analysis
709 showing overall survival of patients from the **(D)** Singapore cohort, **(E)** KUGH & KUCM cohort and
710 **(F)** ACRG cohort stratified based on expression of the downregulated (CAF_down_sig) stromal gene
711 signature. **(G-I)** Enrichment of the CAF_up_sig (mean of normalized counts) in patients with diffuse
712 vs intestinal gastric cancer in the **(G)** Singapore cohort; **(H)** KUGH & KUCM cohort; and **(I)** ACRG
713 cohort. **(J)** Enrichment of the CAF_up_sig and CAF_down_sig (mean of the normalized counts) in
714 patients with mesenchymal phenotype (MP) and epithelial phenotype (EP) subtypes in the KUGH &
715 KUCM cohort (5). **(K)** Enrichment of the CAF_up_sig and CAF_down_sig (mean of normalized
716 counts) in patients with molecular subtypes previously identified in the ACRG cohort (4). One-way
717 ANOVA was used in **(G-K)**.

718
719 **Fig 3. INHBA and THBS1/2 are upregulated in gastric cancer. (A-B)** Gastric cancer was induced
720 in *iLgr5;GLI2A* mice, PDPN⁺ fibroblasts were isolated from the resulting tumors and RNA-seq was
721 performed using fibroblasts isolated from stomachs of naïve mice as control. Signatures comprised of
722 genes upregulated (mCAF_up_sig;) or downregulated (mCAF_down_sig) in PDPN⁺ CAFs vs PDPN⁺
723 normal fibroblasts were derived. **(A)** KM analysis of overall survival in patients from the Singapore
724 cohort stratified based on expression of the mCAF_up_sig (left) or mCAF_down_sig (right). **(B)**
725 Enrichment of the mCAF_up_sig and mCAF_down_sig (mean of normalized counts) in patients with
726 the MP and EP subtypes in the KUGH & KUCM cohort. One-way ANOVA was used for statistical
727 analysis. **(C)** STRING analysis of potential interactions between protein products of genes
728 differentially expressed in gastric cancer patients with favorable vs poor outcome. Proteins with no
729 connections were omitted from the image. THBS2 and INHBA are highlighted in red. **(D-F)** Log
730 normalized counts and p-adjusted values of the indicated genes taken from DESeq analysis of the
731 *iLgr5;GLI2A* PDPN⁺ CAF RNA-seq data (Supplementary Table 8). **(G-I)** Total RNA levels of the
732 indicated genes normalized to HPRT in normal stomachs and tumors (cancer) from *iLgr5;GLI2A* mice.
733 N=3 mice per group, means ± SEM are presented. Two-tailed Student's t-test was used for statistical
734 analysis. **(J-K)** Representative images showing H&E and immunohistochemical staining of the
735 indicated proteins in gastric tumors and control stomachs (naïve) from *iLgr5;GLI2A* mice. N=5 mice
736 for cancer and N=3 mice for normal control. C- cancer, S- stroma. Scale bar- 100 µm. Arrows indicate
737 INHBA and THBS1 positive CAFs.

738

739 **Fig 4. HSF1 is co-expressed with INHBA and THBS1 in human gastric CAFs. (A)** Formalin-fixed
740 paraffin-embedded (FFPE) sections from 64 gastric cancer patients and 4 normal controls were stained
741 by H&E and immunohistochemical staining for HSF1. **(Upper panel)** Images representing high (pt 6)
742 vs low (pt 18) nuclear HSF1 staining in CAFs. **(Lower panel)** Representative images of normal gastric
743 glands and muscle. C- cancer, S- stroma. Scale bar- 100 µm. **(B-C)** 64 gastric cancer samples stained
744 as described above were scored for high/intermediate (int)/low nuclear HSF1 staining in cancer
745 cells/CAF, and KM analysis of overall survival in these patients was performed. **(B)** Patients were
746 stratified by high vs int/low HSF1 scores in cancer cells. **(C)** Patients were stratified by high/int vs low
747 HSF1 scores in CAFs (see Supplementary Table 1). **(D)** FFPE sections from 4 gastric cancer patients
748 and 2 normal stomach controls were stained by multiplexed immunofluorescence for HSF1, INHBA,

749 THBS1 and DAPI (nuclear marker). Representative images from 3 different patients and one control
750 are shown. Scale bar- 50 μ m.

751

752 **Fig 5. Stromal INHBA and THBS1/2 expression is HSF1-dependent.** (A-E) INHBA, THBS1 and
753 THBS2 protein expression levels in WT and *Hsf1* null primary MEFs were analyzed by western blot.
754 Representative blots are shown in (A-B). An arrow indicates the expected size of INHBA bands. (C)
755 INHBA western blot results of 5-10 biological replicates (across 2 experiments) were quantified,
756 normalized to actin and are presented as mean \pm SEM. (D-E) THBS1 western blot results of 5
757 biological replicates (across 2 experiments) and THBS2 western blot results of 5-10 biological
758 replicates (across 3 experiments) were quantified, normalized to actin and are presented as mean \pm
759 SEM. Two-tailed Student's t-test was used for statistical analysis in (C-E). (F-K) WT and *Hsf1* null
760 MEFs were co-cultured with N87-GFP cells for 72h, and each cell type was grown in mono-culture as
761 control. Co-cultures were sorted by flow cytometry using GFP. (F-H) The levels of the indicated genes
762 in (GFP-negative) MEFs were determined by qPCR. Average expression in 6-8 biological replicates
763 (across 3 experiments for *INHBA* and *THBS1* and 2 experiments for *THBS2*), normalized to *HPRT*, \pm
764 SEM are presented. Two-way ANOVA was used for statistical analysis. (I) Representative GFP
765 (upper panel), and brightfield (lower panel) images of mono and co-cultures are shown. N=3
766 biological replicates. Scale bar- 50 μ m. (J) Representative FACS plots showing the percentage of N87-
767 GFP cells co-cultured with WT (left) and *Hsf1* null MEFs (right). N=3 biological replicates. (K) The
768 average percentage (\pm SEM) of N87-GFP cells co-cultured with WT and *Hsf1* null MEFs in 3
769 biological replicates is shown. Two-tailed Student's t-test was used for statistical analysis. (L-N) HFF
770 cells treated with siHSF1, siINHBA, siHSF1-INHBA-THBS2 (siCombined) or siControl as indicated
771 were co-cultured with N87-GFP cells for 72h. The percentage of N87-GFP in the co-cultures averaged
772 across 5-9 biological replicates (\pm SEM) (across 3 experiments for siINHBA and siHSF1-INHBA-
773 THBS2 and 2 experiments for siHSF1) is shown. Two-tailed Student's t-test was used for statistical
774 analysis.

775 **Fig 6. Fibroblast-derived EVs promote tumor growth in an HSF1-dependent manner.** (A) Nude
776 mice were injected subcutaneously with MC38 cancer cells alone, or co-injected with either
777 recombinant THBS2 or Activin A followed by another injection of recombinant protein two days later.
778 Tumor size measured by caliper is presented as mean \pm SEM for N=8 mice per group (across 2
779 experiments). Repeated measures Two-way ANOVA using least-squares means to adjust for group
780 pairwise comparisons was used for statistical analysis. (B-C) Western blot analysis of fractions
781 obtained from Optiprep density gradient isolation of EVs secreted by WT MEFs blotted against
782 exosomal markers ALIX and TSG101, as well as THBS1/2, INHBA and HSF1. EVs from 3 WT MEFs
783 were pooled together for the isolation. The experiment was repeated twice (with different biological
784 replicates), representative results are shown. (D) Representative transmission electron microscope
785 (TEM) images of low (i-ii) and high (iii) density EV fractions (repeated 2 times, from 2 biological
786 replicates). (i) – 1.03% sucrose; (ii) – 1.04% sucrose; (iii) – 1.07% sucrose. Scale bars- 100 nm. (E)
787 Representative western blot showing INHBA levels from EVs isolated from the serum of tumor-
788 bearing and naïve *iLgr5;GLI2A* mice. ALIX was used as loading control. Arrow indicates expected
789 size of ALIX. (F) INHBA levels from EVs isolated from the serum of tumor-bearing and naïve
790 *iLgr5;GLI2A* mice were analyzed using western blot. INHBA levels were normalized to ALIX.
791 Average expression of INHBA normalized to ALIX in 5 biological replicates (across 2 experiments)
792 is presented in as mean \pm SEM. Two-tailed Student's t-test was used for statistical analysis. (G-J)
793 INHBA, THBS1 and THBS2 levels in EVs derived from WT and *Hsf1* null primary MEFs were
794 analyzed using western blot. ALIX and TSG101 were used as loading controls. Representative blots
795 are shown in (G). (H) Average expression of INHBA normalized to TSG101 in 8 biological replicates
796 (across 3 experiments for INHBA) is presented as mean \pm SEM. (I) Average expression of THBS1
797 normalized to TSG101 in 5-7 biological replicates (across 3 experiments) is presented as mean \pm SEM.

798 **(J)** Average expression THBS2 normalized to TSG101 in 10-11 biological replicates (across 4
799 experiments) is presented as mean \pm SEM. Two-tailed Student's t-test was used for statistical analysis
800 in **(H-I)**. **(K)** Nude mice were injected subcutaneously with MC38 cancer cells alone, or co-injected
801 with EVs derived from WT or *Hsf1* null MEFs. Tumor size measured by caliper is presented as mean
802 \pm SEM for N=14-15 mice per group (across 4 experiments). Repeated measures Two-way ANOVA
803 using least-squares means to adjust for group pairwise comparisons was used for statistical analysis.
804 **(L)** Graphic summary of the proposed model. HSF1 in CAFs regulates expression of INHBA and
805 THBS1/2. INHBA and THBS2 from CAFs are packaged into EVs and secreted to the TME, where
806 they are taken up by cancer cells.

807

808

809